



# On the block error rate performance of cooperative non-orthogonal multiple access short-packet communications with full-duplex relay and partial relay selection

Ha Duy Hung<sup>1</sup>  | Hoang Van Toan<sup>2</sup> | Tran Trung Duy<sup>3</sup>  | Le The Dung<sup>4</sup> | Quang Sy Vu<sup>5</sup>

<sup>1</sup>Wireless Communications Research Group, Faculty of Electrical and Electronics Engineering, Ton Duc Thang University, Ho Chi Minh City, Vietnam

<sup>2</sup>Telecommunications University, Nha Trang City, Vietnam

<sup>3</sup>Posts and Telecommunications Institute of Technology, Ho Chi Minh City, Vietnam

<sup>4</sup>Faculty of Computing Fundamentals, FPT University, Ho Chi Minh City, Vietnam

<sup>5</sup>Faculty of Automotive Engineering, School of Technology, Van Lang University, Ho Chi Minh City, Vietnam

## Correspondence

Q. S. Vu, Faculty of Automotive Engineering, School of Technology, Van Lang University, Ho Chi Minh City, Vietnam.

Email: [sy.vq@vlu.edu.vn](mailto:sy.vq@vlu.edu.vn)

## Funding information

Van Lang University, Vietnam

## Abstract

In this paper, we mathematically investigate a downlink non-orthogonal multiple access (NOMA) system for short-packet communications (SPC) in which the near users are used as full-duplex (FD) relays to forward intended signals from the source to a far user. In addition, partial relay selection is employed to enhance the performance of the FD relays under the impact of imperfect interference cancellation. At the far user, selection combining (SC) or maximal ratio combining (MRC) is employed to combine the signals received from the source and the selected FD relay. The analytical expressions for the average block error rate (BLER) of two users over flat Rayleigh fading channels are derived. Furthermore, closed-form asymptotic expressions of the average BLERs at the near and far users in high signal-to-noise ratio (SNR) regimes are obtained. The numerical results show that the analytical BLERs of the near user and far user closely match the simulation results.

## KEYWORDS

block error rate, cooperative NOMA, finite blocklength, full duplex, partial relay selection, short-packet communications

## 1 | INTRODUCTION

Nowadays, the rapid development of mobile communications and the Internet of Things (IoT) offers new requirements and challenges such as massive device connectivity, low latency, and ultra-high reliability for applications in next-generation wireless communications [1]. However, the main restriction of wireless communications studies in the literature is that they assume an arbitrarily low probability of error for infinite transmit blocklengths

based on classical Shannon capacity analysis. Thus, extremely long block lengths are often not pertinent to IoT networks. In this context, short-packet communication (SPC) was first developed in [2] to satisfy stringent delay constraints. In [3], the authors evaluated the average throughput for cooperative IoT networks using SPC. Additionally, from closed-form formula, the authors of [3] solved for both optimal and suboptimal transmission rates to optimize the average throughput. The published study [4] proposed a hybrid automatic repeat request-

based SPC scheme for cooperative IoT networks. The authors of [4] derived closed-form expressions for the average packet error rate and throughput of the proposed scheme over Nakagami- $m$  channels. In [5], the authors studied the security performance of a downlink multicast secure transmission model using full duplex (FD) and SPC, in which a base station could simultaneously send secure signals and receive data signals from users. The authors of [6] considered an SPC-based wireless-powered IoT scheme operating in cognitive radio mode. Furthermore, a deep-learning framework for average block error rate (BLER) prediction was developed in [6]. Feng and others [7] addresses reliability and security issues in SPC networks in the presence of an eavesdropper.

On the other hand, non-orthogonal multiple access (NOMA) is emerging as a potential technology for SPCs because it can support multi-user service with low latency. Sun and others [15] considered a two-user downlink NOMA system in SPC for the first time and pointed out that NOMA significantly outperforms orthogonal multiple access (OMA) in terms of achieving a higher effective throughput subject to the same finite block-length constraint. The analytical expression for the average BLER of a downlink NOMA-SPC system in which all users are uniformly distributed within a disk was derived in [16]. Considering practical applications, where users in a cell may have different quality-of-service (QoS) requirements, the authors in [17] derived analytical expressions for the user-outage probability of a downlink NOMA system with hybrid long-packet communications (for a near user) and SPC (for a far user). In [18], the authors studied the energy-efficiency problem for uplink NOMA-based massive machine-type communications networks using SPC. Combining energy harvesting (EH) and NOMA techniques in SPC, the authors in [8] considered a system consisting of a base station simultaneously communicating with users via an EH relay and derived closed-form analytical expressions for the end-to-end average BLER over Nakagami- $m$  fading channels. For NOMA communication systems, cooperative relaying has been shown to improve the system performance, particularly for far users. Lai and others [9] investigated a two-user downlink NOMA-SPC system in which a near user relays the signals intended for a far user over flat Rayleigh fading channels. However, because the near user operates in half-duplex (HD) mode, it takes two phases to complete a transmission cycle.

Thus far, research on cooperative NOMA relay systems for SPC, where the relay operates in FD mode, is still missing in the literature. Although the authors of [19] studied the BLER performance of both HD and FD relaying schemes, NOMA was not considered. In particular, the authors of [19] analyzed and compared the performance of FD and HD relaying in SPC. Their results

showed that FD relaying was more suitable for systems operating with low transmit power and less stringent BLER requirements. With respect to the combination of NOMA and SPC, the authors of [20] proposed a NOMA downlink system with two users. In addition, the authors of [20] derived expressions for BLER and secure BLER. As proven in [20], an error floor occurs, and the power allocation factors for two users have almost no impact on the secure BLER in high signal-to-noise ratio (SNR) domains. However, a cooperative FD technique was not studied in [20]. By leveraging a wireless-powered relay to extend the transmission range of energy devices, the authors in [11] proposed a downlink system model in which the source node performed NOMA transmission to simultaneously serve two users supported by an HD hybrid relay. Using a dedicated HD relay to support transmission from a base station to two users, the authors in [12] proposed a novel adaptive hybrid relay protocol that mainly focuses on improving the QoS of weak users. In [13], the authors considered a NOMA-SPC scheme using an unmanned aerial vehicle (UAV) that operates as an HD relay to support the communication between a source node and two destination nodes. In addition, the authors of [13] analyzed various performance metrics for the considered scheme, that is, BLER, throughput, latency, and age of information, under imperfect channel state information. In [10], a cooperative NOMA-SPC scheme consisting of a base station, HD relay, and receiver equipped with maximal ratio combining (MRC) or selection combining (SC) was studied. Recently, the authors of [14] evaluated the performance of cooperative FD-NOMA models using SPC, in which BLER expressions for two users were derived. In [14], the authors considered two cases in which the residual self-interference channel at the FD relay was a free fading channel or Rayleigh fading channel. The results obtained in [14] showed that in the high-SNR domain, the BLER performance at the users in these cases was the same. However, only the MRC combiner at the far users was considered in [14]. Although the MRC combiner achieves optimal performance, its implementation, which requires both the amplitude and phase of all channel coefficients, is very complex. Unlike MRC, SC selects only the diversity branch with the highest SNR to decode the received signals [21]. Therefore, the implementation of SC is simpler than that of MRC, and this is the reason why we consider both MRC and SC in this paper. Moreover, the analytical result of BLER at near users in [14] was not highly accurate because the authors used the approximation in [22] (this was proved by the authors of [9]).

Motivated by these observations (see the comparison in Table 1), this paper mathematically analyzes a scenario in which a near user operates in the FD mode and serves as the relay for a far user in the NOMA-SPC

TABLE 1 Comparison of our work and related work.

Relaying/combining techniques	[8]	[9,10]	[11]	[12]	[13]	[14]	Our work
FD relaying	-	-	-	-	-	✓	✓
HD relaying	✓	✓	✓	✓	✓	-	
SC scheme	-	✓	-	✓	-	-	✓
MRC scheme	-	✓	-	-	-	✓	✓

system. In addition, the partial relay selection (PRS) method [23, 24] is also applied to enhance the performance at the near users under the impact of imperfect interference cancellation. To the best of our knowledge, this is the first work related to the combination of PRS, FD relaying, cooperative NOMA-SPC, and MRC/SC equipment at the far user. The main contributions of this article are summarized as follows:

- We first propose the NOMA-SPC cooperative system in which the near user is selected to act as the FD relay node in order to support the performance enhancement for the far user. At the far user, the MRC/SC combiner is employed to enhance the decoding operation. In addition, we perform mathematical modeling for the proposed system to facilitate system analysis.
- We derive analytical expressions of the average BLERs at both users. It is worth noting that we use the approximation method proposed in [9] to obtain more accurate results.
- In order to provide useful insights into the system performance, we also drive the asymptotic closed-form expressions of the average BLERs at high-SNR regimes. Moreover, simulation results are also provided to verify the accuracy of mathematical analysis and to uncover impact of the parameters on the system performance.

The remainder of this paper is organized as follows. The system model of the proposed scheme is described in Section 2. A performance analysis is given in Section 3. Section 4 gives both simulation and theoretical results to verify the obtained results. Finally, the conclusions are presented in Section 5.

## 2 | SYSTEM MODEL

As shown in Figure 1, we consider a cooperative relay system in which base station S transmits the intended signals to two users simultaneously by adopting the NOMA technique (see [9, 25]). There are  $K$  near users, denoted by  $A_1, A_2, \dots, A_K$ , and we denote the selected near relay as A and the far relay as B. Following the NOMA principle, S allocates more transmit power to the

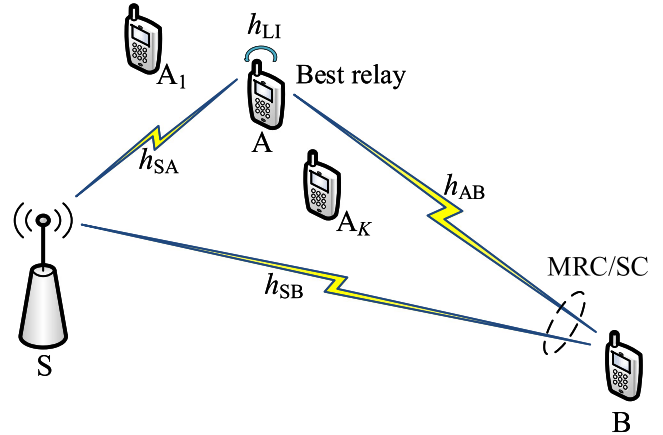


FIGURE 1 Downlink NOMA system model with FD relaying and PRS.

signals of B, and A must decode the signals of B before it can decode its desired signals [9, 25]. All the nodes are equipped with a single antenna. Furthermore, A can perform signal reception and transmission with a single antenna using a circulator [26]. Base station S aims to convey the data of  $N_a$  bits to A and  $N_b$  bits to B by leveraging NOMA over  $m$  channels. User A operates in the FD mode to relay the signals of S to far user B. We assume that all channels are subject to flat Rayleigh fading. Specifically, the channel coefficient between  $\mathcal{X}$  and  $\mathcal{Y}$ , denoted by  $h_{\mathcal{X}\mathcal{Y}}$ , is suffered from Rayleigh fading, where  $X, Y \in \{S, A_k, B\}$ ,  $k = 1, 2, \dots, K$ . With PRS, the best relay A is selected as (see [23, 24])

$$|h_{SA}|^2 = \max_{k=1,2,\dots,K} (|h_{SA_k}|^2), \quad (1)$$

where  $|h_{\mathcal{X}\mathcal{Y}}|^2$  is the channel gain and its expected value is  $\lambda_{\mathcal{X}\mathcal{Y}}$ . Assume that the random variables  $|h_{SA_k}|^2$  are independent and identical, that is,  $\lambda_{SA_k} = \lambda_{SA}$  for all  $k$ .

Next, the transmission powers of S and A are denoted as  $\tilde{P}_S$  and  $\tilde{P}_A$ , respectively. The signal transmitted from S is superposition coded, that is,  $x_S = \sqrt{a_1 \tilde{P}_S} x_A + \sqrt{a_2 \tilde{P}_S} x_B$ , in which  $x_A$  and  $x_B$  are signals intended for A and B, respectively, with expected values  $\mathbb{E}\{x_A^2\} = \mathbb{E}\{x_B^2\} = 1$ . Moreover,  $a_1$  and  $a_2$  are the power allocation coefficients for  $x_A$  and  $x_B$ , respectively, which satisfy  $a_1 > 0$ ,  $a_2 > 0$ , and  $a_1 + a_2 = 1$ . Note that the aim of the proposed system

is to support the QoS for node B and to improve the fairness between nodes. This is the reason why a higher power allocation for the far node B is applied, that is,  $a_1 < a_2$  [27].

Then, the received signal at A can be expressed as

$$y_A = h_{SA} \left( \sqrt{a_1 \tilde{P}_S} x_A + \sqrt{a_2 \tilde{P}_S} x_B \right) + R_{SI} + \omega_A, \quad (2)$$

where  $\omega_A \sim \mathcal{CN}(0, \sigma_A^2)$  denotes the additive white Gaussian noise (AWGN) at A,  $R_{SI}$  is the residual loop self-interference (LI) signal transmitted by A and simultaneously looped back to the receiver. Moreover, after self-interference cancellation is performed in the propagation, analog circuit, and digital domains, self-interference can reach the noise floor [28]. Thus, we assume that  $R_{SI}$  is a Gaussian random variable with a zero mean and variance  $\tilde{P}_A \lambda_{SI}$ , in which  $\lambda_{SI}$  is the LI cancellation coefficient [29].

According to the principle of NOMA decoding, SIC is employed to decode  $x_B$  by treating  $x_A$  as interference. The signal-to-interference-plus-noise ratio (SINR) for decoding  $x_B$  at A is given by

$$\gamma_{x_B}^{SA} = \frac{a_2 \tilde{P}_S |h_{SA}|^2}{a_1 \tilde{P}_S |h_{SA}|^2 + \tilde{P}_A \lambda_{SI} + \sigma_A^2}. \quad (3)$$

As a result, the instantaneous BLER for decoding  $x_B$  at A is represented as [9, 30]

$$\epsilon_{x_B}^{SA} \approx \Psi \left( \gamma_{x_B}^{SA}, N_b, m \right), \quad (4)$$

where  $\Psi(\gamma, N, m) = Q((C(\gamma) - N/m) / \sqrt{V(\gamma)/m})$ ,  $Q(x) = \frac{1}{\sqrt{2\pi}} \int_x^\infty \exp(-t^2/2) dt$ ,  $C(\gamma) = \log_2(1 + \gamma)$  is the Shannon capacity, and  $V(\gamma) = (\log_2(e))^2 (1 - 1/(1 + \gamma)^2)$  is the channel dispersion. Note that the approximation in (4) holds well in SPC when  $m > 100$  [2].

Note that the probability that  $x_B$  is successfully decoded and removed at node A is  $1 - \epsilon_{x_B}^{SA}$ . This probability implies that, in SPCs systems, the perfect SIC cannot be guaranteed. This SIC technique is also used in previous work in SPC [11, 12, 14, 31].

Hence, after successfully decoding  $x_B$ ,  $x_A$  is decoded at A with the SINR determined using

$$\gamma_{x_A}^{SA} = \frac{a_1 \tilde{P}_S |h_{SA}|^2}{\tilde{P}_A \lambda_{SI} + \sigma_A^2}. \quad (5)$$

The instantaneous BLER for decoding  $x_A$  at A is

$$\epsilon_A = \epsilon_{x_B}^{SA} + \left( 1 - \epsilon_{x_B}^{SA} \right) \epsilon_{x_A}^{SA}, \quad (6)$$

where  $\epsilon_{x_A}^{SA} \approx \Psi \left( \gamma_{x_A}^{SA}, N_a, m \right)$ .

The SINR at B for decoding  $x_B$  is similarly given by

$$\gamma_{x_B}^{SB} = \frac{a_2 \tilde{P}_S |h_{SB}|^2}{a_1 \tilde{P}_S |h_{SB}|^2 + \sigma_B^2}, \quad (7)$$

$$\gamma_{x_B}^{AB} = \frac{\tilde{P}_A |h_{AB}|^2}{\sigma_B^2}, \quad (8)$$

where  $\sigma_B^2$  refers to the variance of the AWGN at B.

Exploiting the useful direct link in the FD relaying approach, we consider that B employs both the MRC and SC techniques to combine the received signals. For the MRC scheme, the SINR for decoding  $x_B$  is given as in [32] as

$$\gamma_{x_B}^{MRC} = \gamma_{x_B}^{SB} + \gamma_{x_B}^{AB}. \quad (9)$$

For the SC scheme, the SINR to decode  $x_B$  is

$$\gamma_{x_B}^{SC} = \max \left( \gamma_{x_B}^{SB}, \gamma_{x_B}^{AB} \right). \quad (10)$$

Consequently, the instantaneous BLERs for decoding  $x_B$  at B using the SC and MRC techniques are, respectively, given by [33]

$$\epsilon_B^C = \epsilon_{x_B}^{SA} \epsilon_{x_B}^{SB} + \left( 1 - \epsilon_{x_B}^{SA} \right) \epsilon_{x_B}^C, \quad (11)$$

where  $C \in \{\text{SC}, \text{MRC}\}$ ,  $\epsilon_{x_B}^{SB} \approx \Psi \left( \gamma_{x_B}^{SB}, N_b, m \right)$ , and  $\epsilon_{x_B}^C \approx \Psi \left( \gamma_{x_B}^C, N_b, m \right)$ .

### 3 | PERFORMANCE ANALYSIS

In this section, we focus on deriving the expressions for the BLERs at A and B for both the SC and MRC schemes. As mentioned in [16], the derived average BLER does not depend on the actual encoding and modulation techniques.

#### 3.1 | Average BLER needed to decode $x_A$ at A

Without loss of generality, we assume  $\sigma_A^2 = \sigma_B^2 = \sigma^2$  throughout this paper. In addition, for the convenience of mathematical analysis, we set  $P_S = \tilde{P}_S / \sigma^2$  and  $P_A = \tilde{P}_A / \sigma^2$ .

From (6), the average BLER needed to decode  $x_A$  at A can be calculated as

$$\mathbb{E}\{\epsilon_A\} = \mathbb{E}\left\{ \epsilon_{x_B}^{SA} \right\} + \mathbb{E}\left\{ \epsilon_{x_A}^{SA} \right\} - \mathbb{E}\left\{ \epsilon_{x_A}^{SA} \epsilon_{x_B}^{SA} \right\}. \quad (12)$$

The first two terms on the right side of  $\mathbb{E}\{\epsilon_{x_Y}^{SA}\}$  in (12) can be approximated as

$$\mathbb{E}\{\epsilon_{x_Y}^{SA}\} \approx \int_0^{\infty} \Psi(\gamma_{x_Y}^{SA}, N_y, m) f_{\gamma_{x_Y}^{SA}}(x) dx, \quad (13)$$

where  $Y \in \{A, B\}$ ,  $y \in \{a, b\}$ , and  $f_X(x)$  denotes the PDF of  $X$ . Moreover, from [9, 30], we have  $\Psi(\gamma_{x_Y}^{SA}, N_y, m) \approx Z_{N_y, m}(\gamma)$  with

$$Z_{N_y, m}(\gamma) = \begin{cases} 1, & \gamma \leq v_y, \\ \frac{1}{2} - \delta_y \sqrt{m}(\gamma - \beta_y), & v_y \leq \gamma < u_y, \\ 0, & \gamma > u_y, \end{cases} \quad (14)$$

where  $\beta_y = 2^{N_y/m} - 1$ ,  $\delta_y = 1/\sqrt{2\pi(2^{2N_y/m} - 1)}$ ,  $v_y = \beta_y - (1/2\delta_y\sqrt{m})$ , and  $u_y = \beta_y + (1/2\delta_y\sqrt{m})$ .

Substituting (14) into (13), we obtain (see [9, 30])

$$\mathbb{E}\{\epsilon_{x_Y}^{SY}\} \approx \delta_y \sqrt{m} \int_{v_y}^{u_y} F_{\gamma_{x_Y}^{SA}}(x) dx, \quad (15)$$

where  $F_X(x)$  denotes the cumulative distribution function (CDF) of  $X$ .

**Theorem 1.** In the FD-NOMA cooperative relay system considered for SPC, the average BLER of  $x_A$  at A is given by

$$\mathbb{E}\{\epsilon_A\} \approx \mathbb{E}\{\epsilon_{x_B}^{SA}\} + \mathbb{E}\{\epsilon_{x_A}^{SA}\} - \min\left(\mathbb{E}\{\epsilon_{x_B}^{SA}\}, \mathbb{E}\{\epsilon_{x_A}^{SA}\}\right), \quad (16)$$

in which  $\mathbb{E}\{\epsilon_{x_A}^{SA}\}$  is given as

$$\mathbb{E}\{\epsilon_{x_A}^{SA}\} \approx 1 + \sum_{q=1}^K (-1)^q C_K^q \frac{\delta_a \sqrt{m}}{q\phi_a} (e^{-qv_a\phi_a} - e^{-qu_a\phi_a}), \quad (17)$$

and  $\mathbb{E}\{\epsilon_{x_B}^{SA}\}$  is computed for three cases as follows:

Case 1:  $u_b \leq u$ .

$$\begin{aligned} \mathbb{E}\{\epsilon_{x_B}^{SA}\} &\approx 1 + \sum_{q=1}^K (-1)^q C_K^q \delta_b \sqrt{m} e^{q\phi_a} \\ &\quad \times \left[ (u - v_b) e^{\frac{q\phi_a u}{u-v_b}} - (u - u_b) e^{\frac{q\phi_a u}{u-u_b}} \right] \\ &\quad + \sum_{q=1}^K (-1)^q C_K^q \delta_b \sqrt{m} q \phi_a u e^{q\phi_a} \\ &\quad \times \left[ \text{Ei}\left(\frac{q\phi_a u}{v_b - u}\right) - \text{Ei}\left(\frac{q\phi_a u}{u_b - u}\right) \right], \end{aligned} \quad (18)$$

Case 2:  $v_b \leq u < u_b$ .

$$\begin{aligned} \mathbb{E}\{\epsilon_{x_B}^{SA}\} &\approx 1 + \sum_{q=1}^K (-1)^q C_K^q \delta_b \sqrt{m} e^{q\phi_a} \\ &\quad \times \left[ (u - v_b) e^{\frac{q\phi_a u}{u-v_b}} + q\phi_a u \text{Ei}\left(\frac{q\phi_a u}{v_b - u}\right) \right], \end{aligned} \quad (19)$$

• Case 3:  $u < v_b$

$$\mathbb{E}\{\epsilon_{x_B}^{SA}\} \approx 1, \quad (20)$$

where  $\phi_a = (P_A \lambda_{SI} + 1)/(P_S a_1 \lambda_{SA})$ ,  $u = a_2/a_1$ ,  $\text{Ei}(\cdot)$  denotes the exponential integral function [34, Eq. (8.211)], and  $C_K^q = K!/q!(K-q)!$  is a binomial coefficient.

*Proof.* Applying Proposition 1 in [9], the third term on the right side of (12) can be expressed as

$$\mathbb{E}\{\epsilon_{x_A}^{SA} \epsilon_{x_B}^{SA}\} \approx \min\left(\mathbb{E}\{\epsilon_{x_A}^{SA}\}, \mathbb{E}\{\epsilon_{x_B}^{SA}\}\right). \quad (21)$$

Next, using the results obtained in (A.3), (A.5), (A.8), and (A.10), the proof of Theorem 1 is completed.  $\square$

### 3.2 | Average BLER needed to decode $x_B$ at B with SC

**Theorem 2.** The average BLER of  $x_B$  in the proposed scheme with the SC combiner at node B can be expressed by

$$\begin{aligned} \mathbb{E}\{\epsilon_{x_B}^{SC}\} &= \mathbb{E}\{\epsilon_{x_B}^{SA}\} \mathbb{E}\{\epsilon_{x_B}^{SB}\} \\ &\quad + \left(1 - \mathbb{E}\{\epsilon_{x_B}^{SA}\}\right) \mathbb{E}\{\epsilon_{x_B}^{SB}\} \mathbb{E}\{\epsilon_{x_B}^{AB}\}, \end{aligned} \quad (22)$$

where  $\mathbb{E}\{\epsilon_{x_B}^{SA}\}$  is given in (18)–(20) and  $\mathbb{E}\{\epsilon_{x_B}^{SB}\}$  and  $\mathbb{E}\{\epsilon_{x_B}^{AB}\}$  are given in (25) and (26), respectively.

*Proof.* From (11), the average BLER needed to decode  $x_B$  at B using the SC scheme can be calculated as

$$\mathbb{E}\{\epsilon_B^{SC}\} = \mathbb{E}\{\epsilon_{x_B}^{SA}\} \mathbb{E}\{\epsilon_{x_B}^{SB}\} + \left(1 - \mathbb{E}\{\epsilon_{x_B}^{SA}\}\right) \mathbb{E}\{\epsilon_{x_B}^{SC}\}. \quad (23)$$

Now, we obtain the approximation expression of  $\mathbb{E}\{\epsilon_{x_B}^{SB}\}$ . From (7), we can express CDF of  $\gamma_{x_B}$  as

$$\begin{aligned}
F_{\gamma_{x_B}^{SB}}(x) &= \Pr \left( \frac{a_2 P_S |h_{SB}|^2}{a_1 P_S |h_{SB}|^2 + 1} < x \right) \\
&= \begin{cases} \Pr \left( |h_{SB}|^2 < \frac{x}{Pa_1(u-x)} \right), & \text{if } x < u \\ 1, & \text{if } x \geq u \end{cases} \quad (24) \\
&= \begin{cases} 1 - e^{-\frac{\phi_b x}{u-x}}, & \text{if } x < u \\ 1, & \text{if } x \geq u, \end{cases}
\end{aligned}$$

where  $\phi_b = 1/P_S a_1 \lambda_{SB}$ .

Note that the CDF expression of  $\gamma_{x_B}^{SB}$  in (24) has the same form as the expression of the CDF of  $\gamma_{x_B}^{SA}$  in (A.4). Substituting the CDF of  $\gamma_{x_B}^{SB}$  in (15) and performing the same analysis steps as when calculating  $\mathbb{E}\{\epsilon_{x_B}^{SA}\}$ , we obtain the approximation expression of  $\mathbb{E}\{\epsilon_{x_B}^{SB}\}$  as in (25).

$$\mathbb{E}\{\epsilon_{x_B}^{SB}\} \approx \begin{cases} 1 - \delta_b \sqrt{m} e^{\phi_b} \phi_b u \left( \text{Ei} \left( \frac{\phi_b u}{v_b - u} \right) - \text{Ei} \left( \frac{\phi_b u}{u_b - u} \right) \right) - \delta_b \sqrt{m} e^{\phi_b} \left( (v_b - u) e^{\frac{\phi_b u}{v_b - u}} - (u_b - u) e^{\frac{\phi_b u}{u_b - u}} \right), & \text{if } u_b < u, \\ 1 - \delta_b \sqrt{m} e^{\phi_b} \phi_b u \left( \text{Ei} \left( \frac{\phi_b u}{v_b - u} \right) + \frac{v_b - u}{\phi_b u} e^{\frac{\phi_b u}{v_b - u}} \right), & \text{if } v_b < u < u_b, \\ 1, & \text{if } u < v_b. \end{cases} \quad (25)$$

Next, using a similar method for deriving  $\mathbb{E}\{\epsilon_{x_A}^{SA}\}$ , we can calculate  $\mathbb{E}\{\epsilon_{x_B}^{AB}\}$  as

$$\mathbb{E}\{\epsilon_{x_B}^{AB}\} \approx 1 - \delta_b \sqrt{m} P_A \lambda_{AB} \left( e^{-\frac{v_b}{P_A \lambda_{AB}}} - e^{-\frac{u_b}{P_A \lambda_{AB}}} \right). \quad (26)$$

In order to obtain the average BLER of  $x_B$  at B, we need to find the expression of  $\mathbb{E}\{\epsilon_{x_B}^{SC}\}$ . Note that when  $m$  is sufficiently large,  $\mathbb{E}\{\epsilon_{x_B}^{SC}\}$  can be approximated as  $\mathbb{E}\{\epsilon_{x_B}^{SB}\} \mathbb{E}\{\epsilon_{x_B}^{AB}\}$  [9]. Therefore, the proof of Theorem 2 is complete.  $\square$

### 3.3 | Average BLER needed to decode $x_B$ at B with MRC

**Theorem 3.** The average BLER of  $x_B$  in the proposed scheme using the MRC combiner is given by

$$\mathbb{E}\{\epsilon_B^{\text{MRC}}\} = \mathbb{E}\{\epsilon_{x_B}^{\text{SA}}\} \mathbb{E}\{\epsilon_{x_B}^{\text{SB}}\} + \left( 1 - \mathbb{E}\{\epsilon_{x_B}^{\text{SA}}\} \right) \mathbb{E}\{\epsilon_{x_B}^{\text{MRC}}\}, \quad (27)$$

where  $\mathbb{E}\{\epsilon_{x_B}^{\text{SA}}\}$  is given in (18)–(20) and  $\mathbb{E}\{\epsilon_{x_B}^{\text{SB}}\}$  and  $\mathbb{E}\{\epsilon_{x_B}^{\text{MRC}}\}$  are given in (25) and (31), respectively.

*Proof.* From (11), the average BLER needed to decode  $x_B$  at B using MRC can be calculated as

$$\mathbb{E}\{\epsilon_{x_B}^{\text{MRC}}\} = \mathbb{E}\{\epsilon_{x_B}^{\text{SA}}\} \mathbb{E}\{\epsilon_{x_B}^{\text{SB}}\} + \left( 1 - \mathbb{E}\{\epsilon_{x_B}^{\text{SA}}\} \right) \mathbb{E}\{\epsilon_{x_B}^{\text{MRC}}\}. \quad (28)$$

In order to derive the analytical expression of  $\mathbb{E}\{\epsilon_{x_B}^{\text{MRC}}\}$ , we need to find the expression of  $\gamma_{x_B}^{\text{MRC}}$ . First, we compute  $F_{\gamma_{x_B}^{\text{MRC}}}(\gamma)$ , which is the CDF of  $\gamma_{x_B}^{\text{MRC}}$  as

$$\begin{aligned}
F_{\gamma_{x_B}^{\text{MRC}}}(\gamma) &= \Pr \left( \frac{a_2 P_S |h_{SB}|^2}{a_1 P_S |h_{SB}|^2 + 1} + P_A |h_{AB}|^2 < \gamma \right) \\
&= \int_0^{\frac{\gamma}{P_A}} \Pr \left( |h_{SB}|^2 < \frac{\gamma - P_A y}{P_S [a_2 - a_1(\gamma - P_A y)]} \right) f_{|h_{AB}|^2}(y) dy. \quad (29)
\end{aligned}$$

Then, we have the expression of  $F_{\gamma_{x_B}^{\text{MRC}}}(\gamma)$  for two cases, that is,

$$F_{\gamma_{x_B}^{\text{MRC}}}(\gamma) = \begin{cases} F_{\gamma_{x_B}^{\text{MRC}}}^L(\gamma) & \text{if } \gamma < u \\ F_{\gamma_{x_B}^{\text{MRC}}}^H(\gamma) & \text{if } \gamma > u \end{cases} \quad (30)$$

where  $F_{\gamma_{x_B}}^L(\gamma)$  and  $F_{\gamma_{x_B}}^H(\gamma)$  are given in (B.2) and (B.4) in Appendix B, respectively. Then, we have

$$\mathbb{E}\left\{\epsilon_{x_B}^{\text{MRC}}\right\} = \begin{cases} E_{x_B}^1 & \text{if } u > u_b \\ E_{x_B}^2 & \text{if } u < v_b \\ E_{x_B}^3 & \text{if } v_b < u < u_b \end{cases}, \quad (31)$$

where

$$E_{x_B}^1 \approx \delta_b \sqrt{m} \int_{v_b}^{u_b} F_{\gamma_{x_B}}^L(\gamma) d\gamma, \quad (32)$$

$$E_{x_B}^2 \approx \delta_b \sqrt{m} \int_{v_b}^{u_b} F_{\gamma_{x_B}}^H(\gamma) d\gamma, \quad (33)$$

and

$$E_{x_B}^3 \approx \delta_b \sqrt{m} \int_{v_b}^u F_{\gamma_{x_B}}^H(\gamma) d\gamma + \delta_b \sqrt{m} \int_u^{u_b} F_{\gamma_{x_B}}^L(\gamma) d\gamma. \quad (34)$$

Substituting (B.2) into  $E_{x_B}^1$  and applying the Gaussian–Chebyshev quadrature approach, we obtain (35), where  $y_j = \cos\left(\frac{2j-1}{2N}\pi\right)$ ,  $x_j = \frac{1}{2}\delta_b\sqrt{m}y_j + \beta_b$ ,  $y_i = \cos\left(\frac{2i-1}{2N}\pi\right)$ , and  $N$  is a complexity-accuracy trade-off parameter.

Next, substituting (B.4) into  $E_{x_B}^2$  and performing some algebraic manipulations yield

$$E_{x_B}^2 \approx 1 - \delta_b \sqrt{m} P_A \left( \lambda_{AB} + e^{\frac{1}{P_S a_1 \lambda_{SB}} + \frac{u}{P_A \lambda_{AB}}} \eta \right) \left( e^{-\frac{v_b}{P_A \lambda_{AB}}} - e^{-\frac{u_b}{P_A \lambda_{AB}}} \right). \quad (36)$$

Similarly, substituting (B.2) and (B.4) into  $E_{x_B}^3$ , after some calculations, we obtain  $E_{x_B}^3$  as in (37), where  $y_k = \cos\left(\frac{2k-1}{2K}\pi\right)$ ,  $x_k = \frac{1}{2}\delta_b\sqrt{m}y_k + \delta_b$ , and  $K$  is a complexity-accuracy trade-off parameter.

Substituting (35), (36), and (37) into (31), we obtain the closed-form expression of  $\mathbb{E}\left\{\epsilon_{x_B}^{\text{MRC}}\right\}$ .  $\square$

#### 4 | ASYMPTOTIC AVERAGE BLER

To provide insights into the system performance, we derive asymptotic closed-form expressions of the BLERs at A and B at high transmit power, that is,  $P_S, P_A \rightarrow +\infty$ . In addition, we fix  $P_A = \mu P_S$ , where  $\mu$  is a positive constant. From (5), we can approximate the BLER at high transmit power as

$$\gamma_{x_A}^{\text{SA}} \approx \frac{a_1 \tilde{P}_S |h_{\text{SA}}|^2}{\tilde{P}_A \lambda_{\text{SI}}} = \frac{a_1 |h_{\text{SA}}|^2}{\mu \lambda_{\text{SI}}}. \quad (38)$$

$$E_{x_B}^1 \approx 1 - \delta_b \sqrt{m} P_A \lambda_{AB} \left( e^{-\frac{v_b}{P_A \lambda_{AB}}} - e^{-\frac{u_b}{P_A \lambda_{AB}}} \right) - \frac{1}{4P_A \lambda_{AB}} \sum_{i=1}^N w_N \sqrt{1-y_i^2} \sum_{j=1}^N w_N \sqrt{1-y_j^2} x_j \exp \left( \frac{x_j(y_i-1)}{P_S a_1 \lambda_{SB} [x_j(y_i-1) + 2u]} - \frac{x_j(y_i+1)}{2P_A \lambda_{AB}} \right). \quad (35)$$

$$E_{x_B}^3 \approx 1 + \delta_b \sqrt{m} \left( (u - v_b) - P_A \lambda_{AB} \left( e^{-\frac{u}{P_A \lambda_{AB}}} - e^{-\frac{u_b}{P_A \lambda_{AB}}} \right) \right) - \frac{1 + \frac{\eta e^{\frac{1}{P_S a_1 \lambda_{SB}} + \frac{u}{P_A \lambda_{AB}}}}{\lambda_{AB}}}{P_A \lambda_{AB}} \left( e^{-\frac{v_b}{P_A \lambda_{AB}}} - e^{-\frac{u_b}{P_A \lambda_{AB}}} \right) - \frac{\delta_b \sqrt{m}}{2P_A \lambda_{AB}} \sum_{i=1}^N w_N \sqrt{1-y_i^2} \sum_{k=1}^K w_K \sqrt{1-y_k^2} x_k \exp \left( \frac{x_k(y_i-1)}{P_S a_1 \lambda_{SB} [x_k(y_i-1) + 2u]} - \frac{x_k(y_i+1)}{2P_A \lambda_{AB}} \right), \quad (37)$$

Using (38) in the same manner as deriving  $\mathbb{E}\{\epsilon_{x_A}^{SA}\}$  in (17), we obtain the following result:

$$\begin{aligned} \mathbb{E}\{\epsilon_{x_A}^{SA}\} &\approx \mathbb{E}\{\epsilon_{x_A}^{SA,\infty}\} \\ &\approx 1 + \sum_{q=1}^K (-1)^q C_K^q \frac{\delta_a \sqrt{m}}{q\phi_a^*} (e^{-qv_a\phi_a^*} - e^{-qu_a\phi_a^*}), \end{aligned} \quad (39)$$

where  $\phi_a^* = \mu\lambda_{SI}/(a_1\lambda_{SA})$ .

Similarly, we approximate  $\mathbb{E}\{\epsilon_{x_B}^{SA}\}$  in (18)–(20) as follows:

$$\mathbb{E}\{\epsilon_{x_B}^{SA}\} \approx \begin{cases} \mathbb{E}\{\epsilon_{x_{B,1}}^{SA,\infty}\}, & \text{if } u_b \leq u, \\ \mathbb{E}\{\epsilon_{x_{B,2}}^{SA,\infty}\}, & \text{if } v_b \leq u < u_b, \\ 1, & \text{if } v_b \leq u, \end{cases} \quad (40)$$

where  $\mathbb{E}\{\epsilon_{x_{B,1}}^{SA,\infty}\}$  and  $\mathbb{E}\{\epsilon_{x_{B,2}}^{SA,\infty}\}$  are given in (41) and (42).

$$\begin{aligned} E_{x_B}^3 &\approx 1 + \delta_b \sqrt{m} \left( (u - v_b) - P_A \lambda_{AB} \left( e^{-\frac{u}{P_A \lambda_{AB}}} - e^{-\frac{u_b}{P_A \lambda_{AB}}} \right) \right) \\ &\quad - \left( 1 + \frac{\eta e^{\frac{1}{P_S a_1 \lambda_{AB}} + \frac{u}{P_A \lambda_{AB}}}}{\lambda_{AB}} \right) P_A \lambda_{AB} \left( e^{-\frac{v_b}{P_A \lambda_{AB}}} - e^{-\frac{u}{P_A \lambda_{AB}}} \right) \\ &\quad - \frac{\delta_b \sqrt{m}}{2P_A \lambda_{AB}} \sum_{i=1}^N w_N \sqrt{1 - \gamma_i^2} \sum_{k=1}^K w_K \sqrt{1 - \gamma_k^2} x_k \exp \\ &\quad \left( \frac{x_k (y_i - 1)}{P_S a_1 \lambda_{SB} [x_k (y_i - 1) + 2u]} - \frac{x_k (y_i + 1)}{2P_A \lambda_{AB}} \right), \end{aligned} \quad (41)$$

$$\begin{aligned} \mathbb{E}\{\epsilon_{x_{B,2}}^{SA,\infty}\} &= 1 + \sum_{q=1}^K (-1)^q C_K^q \delta_b \sqrt{m} e^{q\phi_a^*} \left[ (u - v_b) e^{-\frac{q\phi_a^* u}{u - v_b}} \right. \\ &\quad \left. + q\phi_a^* u \text{Ei} \left( \frac{q\phi_a^* u}{v_b - u} \right) \right]. \end{aligned} \quad (42)$$

*Remark 1.* Substituting (40), (41), and (42) into (16), we obtain the asymptotic closed-form formulas of  $\mathbb{E}\{\epsilon_A\}$  at a high transmit power. Moreover, it is worth noting that these asymptotic expressions do not depend on  $P_S, P_A$ , which means that the diversity order obtained at A is zero.

Next, we use the first-order Riemann integral approximation, that is,  $\int_{v_i}^{u_i} f(x) dx \approx (u_i - v_i) f((u_i + v_i)/2)$ . Note that

when  $m$  is sufficiently large, the integral interval  $[v_i, u_i]$ ,  $i \in \{a, b\}$ , is small, and  $f(\cdot)$  is an exponential function (see A.5) that is integrable and continuous in  $[v_i, u_i]$ . Moreover, using the property that  $e^{-x} \approx 1 - x$  for small  $x$ , from (15) and (24), we have

$$\begin{aligned} \mathbb{E}\{\epsilon_{x_B}^{SB}\} &\approx \delta_y \sqrt{m} \int_{v_b}^{u^*} F_{\gamma_{x_B}^{SB}}(x) dx \\ &\approx \delta_y \sqrt{m} (u^* - v_b) F_{\gamma_{x_B}^{SB}} \left( \frac{u^* + v_b}{2} \right) \\ &\approx \delta_y \sqrt{m} (u^* - v_b) \left[ 1 - e^{-\frac{\phi_b (u^* + v_b)}{2u - (u^* + v_b)}} \right] \\ &\approx \delta_y \sqrt{m} \frac{\phi_b (u^* - v_b) (u^* + v_b)}{2u - (u^* + v_b)} \\ &\approx \begin{cases} \frac{\phi_b \beta_b}{u - \beta_b}, & \text{if } u_b \leq u \\ \delta_y \sqrt{m} \phi_b (v_b + u), & \text{if } v_b \leq u < u_b, \\ 1, & \text{if } u < v_b \end{cases} \end{aligned} \quad (43)$$

where  $u^* \in \{u, u_b\}$ .

In the same manner, it is straightforward to obtain

$$\mathbb{E}\{\epsilon_{x_B}^{AB}\} \approx \frac{\beta_b}{P_A \lambda_{AB}}. \quad (44)$$

Substituting (40)–(42), (43), and (44) into (22), we obtain the asymptotic closed-form expressions of BLER at B when the SC combiner is used.

Next, we attempt to find the approximate formulas for  $\mathbb{E}\{\epsilon_{x_B}^{MRC}\}$ . First, we have to approximate the CDF  $F_{\gamma_{x_B}^{MRC}}(\gamma)$  in (30) at high transmit power as follows:

Case 1:  $\gamma < u$ .

First, we rewrite CDF  $F_{\gamma_{x_B}^{MRC}}^L(\gamma)$  in (B.1) as

$$\begin{aligned} F_{\gamma_{x_B}^{MRC}}^L(\gamma) &= \int_0^{\frac{\gamma}{P_A}} \left( 1 - e^{-\frac{\phi_b (\gamma - P_A y)}{u + P_A y - \gamma}} \right) \frac{1}{\lambda_{AB}} e^{-\frac{\gamma}{\lambda_{AB}} y} dy \\ &= \int_0^1 \left( 1 - e^{-\frac{\phi_b (\gamma - \gamma t)}{u - \gamma + \gamma t}} \right) \frac{\gamma}{P_A \lambda_{AB}} e^{-\frac{\gamma t}{P_A \lambda_{AB}}} dt \\ &= \int_0^1 G(t) dt, \end{aligned} \quad (45)$$

where



$$G(t) = \left(1 - e^{-\frac{\phi_b(\gamma-\gamma t)}{u-\gamma+\gamma t}}\right) \frac{\gamma}{P_A \lambda_{AB}} e^{-\frac{\gamma t}{P_A \lambda_{AB}}}. \quad (46)$$

Next, at high transmit power, we can approximate  $G(t)$  as

$$G(t) \approx \frac{\phi_b \gamma^2}{P_A \lambda_{AB} u} (1-t). \quad (47)$$

Substituting (47) into (46), an approximate expression for  $F_{\gamma_{x_B}}^L(\gamma)$  can be given as

$$F_{\gamma_{x_B}}^L(\gamma) \approx \frac{\phi_b}{P_A \lambda_{AB}} \frac{\gamma^2}{2u}. \quad (48)$$

- Case 2:  $\gamma > u$ .

In this case, we first approximate the SINR obtained at B in (9) at high transmit power as

$$\gamma_{x_B}^{\text{MRC}} = \frac{a_2 P_S |h_{SB}|^2}{a_1 P_S |h_{SB}|^2 + 1} + P_A |h_{AB}|^2 \approx P_A |h_{AB}|^2 + u. \quad (49)$$

Therefore, the CDF  $F_{\gamma_{x_B}}^H(\gamma)$  can be approximated as

$$\begin{aligned} F_{\gamma_{x_B}}^H(\gamma) &\approx \Pr(P_A |h_{AB}|^2 + u < \gamma) = 1 - e^{-\frac{\gamma-u}{P_A \lambda_{AB}}} \\ &\approx \frac{\gamma-u}{P_A \lambda_{AB}}. \end{aligned} \quad (50)$$

From (48) and (50),  $\mathbb{E}\{\epsilon_{x_B}^{\text{MRC}}\}$  can be approximated as follows:

$$\mathbb{E}\{\epsilon_{x_B}^{\text{MRC}}\} = \begin{cases} E_{x_B}^{1,\infty}, & \text{if } u > u_b, \\ E_{x_B}^{2,\infty}, & \text{if } u < v_b, \\ E_{x_B}^{3,\infty}, & \text{if } v_b < u < u_b, \end{cases} \quad (51)$$

where

$$\begin{aligned} E_{x_B}^{1,\infty} &= \frac{\phi_b}{P_A \lambda_{AB}} \frac{(u_b^2 + u_b v_b + v_b^2)}{6u}, E_{x_B}^{2,\infty} = \frac{u_b + v_b - 2u}{2P_A \lambda_{AB}}, \\ E_{x_B}^{3,\infty} &= \frac{\delta_b \sqrt{m}}{P_A \lambda_{AB}} \left[ \frac{\phi_b}{6u} (u^3 - v_b^3) + \frac{(u_b - u)^2}{2} \right]. \end{aligned} \quad (52)$$

Substituting (40)–(42), (43), and (51)–(52) into (28), we obtain the asymptotic closed-form expressions of BLER at B when the MRC combiner is used.

## 5 | SIMULATION RESULTS

In this section, numerical results are provided to verify the proposed derivation approach and evaluate the average BLER of the considered system. For illustration purpose only, we designed the system parameters as follows:  $\lambda_{SA} = -80$  dBm,  $\lambda_{SB} = -85$  dBm,  $\lambda_{AB} = -87$  dBm,  $\lambda_{SI} = -60$  dB,  $N_a = 300$ ,  $N_b = 100$ , and the variance of AWGN is  $\sigma^2 = -114$  dBm. It is worth noting that the derived expressions can be applied for all the practical values of the system parameters.

Figure 2 plots the simulation results (Sim) and theoretical results (Theory) of the average BLERs at A and B versus  $\tilde{P}_S$ . We can see that the simulation and theoretical results for the BLERs at A and B are in good agreement. In addition, at a high transmit power (or high transmit SNR), the BLER curves converge to the approximate ones (High SNR). It is also clear that the BLER performance at both A and B is better when the transmit powers  $\tilde{P}_S$  and  $\tilde{P}_A$  increase. However, as proven in Section 4, BLER at A at high transmit power regimes does not depend on  $\tilde{P}_S$ , and hence, the obtained diversity order is zero. In contrast to A, B obtains a diversity order of 2, that is, slopes of the BLER curves are equal to 2 in both cases where MRC and SC are used at B. Figure 2 also shows that BLER at B is lower when the MRC technique is used. Due to the diversity gain, the BLER performance at B is better than that at A at a high transmit power. However,

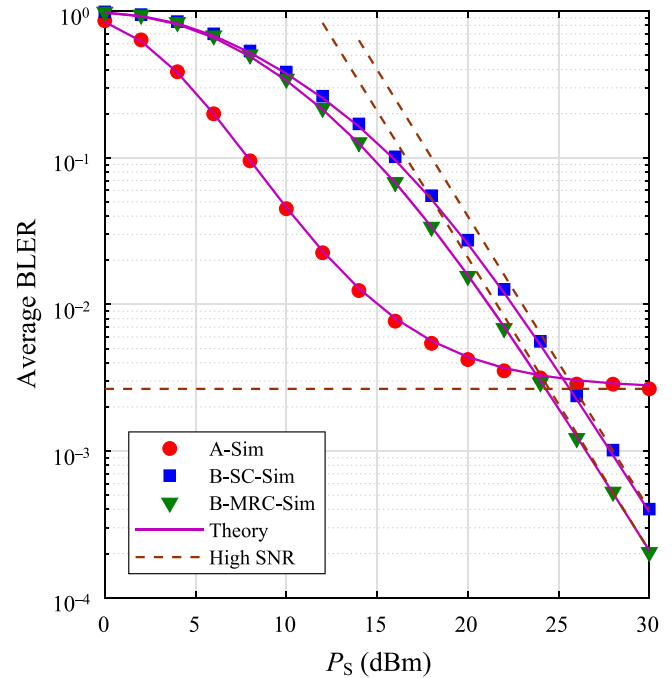


FIGURE 2 Average BLER at A and B as a function of  $\tilde{P}_S$  in dBm when  $\mu = 0.05$ ,  $a_2 = 0.9$ ,  $m = 200$ ,  $K = 3$ .

in this figure, the BLER at A is lower than those at B at low and medium values of  $\tilde{P}_S$ .

In Figure 3, we present the average BLERs at A and B versus  $\tilde{P}_S$ . For ease of observation, the asymptotic results of BLERs at B are not presented in Figure 3. Similarly, the simulation results closely match the theoretical ones, and at a high transmit power, the BLER curves of A converge to the floor values, and those of B obtain the slope of 2. In Figure 3, the BLER performance of A with  $K = 4$  is much better than that with  $K = 1$ . Note that the scheme with  $K = 1$  is equivalent to one using the random relay selection method (or one without using the relay selection method). Therefore, the PRS method provides better performance for the selected near user. However, as we can see from Figure 3, the BLER performance of B only slightly changes in the two cases of  $K = 1$  and  $K = 4$ .

Figure 4 presents the average BLERs at A and B as a function of the number of near relays ( $K$ ). We can see that the BLER performance of A significantly decreases as  $K$  increases, and A obtains better performance than B when  $K$  is higher than 3. Observing the BLERs at B, we can see that the BLER values only slightly decrease as  $K$  increases from 1 to 2, and with  $K \geq 2$ , the BLER performance at B remains almost unchanged. Indeed, from (11), we can observe that as  $K \geq 2$ ,  $\epsilon_{x_B}^{SA} \approx 0$ , and hence,  $\epsilon_B^C \approx \epsilon_{x_B}^C$ . Because  $\epsilon_{x_B}^C$  depends only on the quality of the S–B and A–B links, this is the reason why the BLERs at B only change slightly as  $K$  increases. From Figures 3 and 4, we

can conclude that the PRS method only enhances the performance for the near users.

Figure 5 shows the impact of the power allocation factor  $a_2$  on the BLER performance at A and B for different values of  $m$ . We first observe that as  $a_2$  increases, the BLER values at A significantly increase but those at B slightly decrease. This is due to the fact that when  $a_2$  is high, the transmit power allocated to the signals of the nodes A and B is lower and higher, respectively. Therefore, the performances of A and B are lower and higher, respectively. Moreover, because node A suffers from self-interference, its performance significantly degrades as  $a_2$  increases. In practice, the value of  $a_2$  must be designed carefully to obtain the required QoS. For example, if the required QoS is that the BLERs at A and B are lower than 0.001, with  $m = 170$  and MRC is used at B, then, from Figure 5, the appropriate value of  $a_2$  should be in the interval (0.75, 0.79). Figure 5 also shows that the BLER performance at A and B is better with higher values of  $m$ .

Figure 6 shows the impact of the transmit power of node A on the BLER performance. In particular, this figure presents the average BLERs at A and B as a function of  $\mu$ . As observed, as  $\mu$  increases, the BLER values at A and B increase and decrease, respectively. This is due to the fact that with higher value of  $\mu$  (or higher  $\tilde{P}_A$ ), node A suffers from higher interference because of its FD transmission. On the other hand, with higher transmit power  $\tilde{P}_A$ , the performance of B is better because SINR of

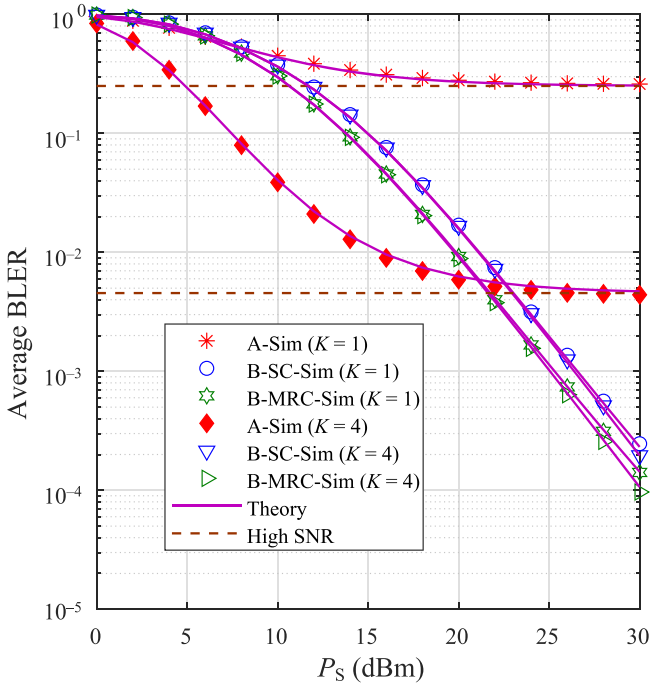


FIGURE 3 Average BLER at A and B as a function of  $\tilde{P}_S$  in dBm when  $\mu = 0.1$ ,  $a_2 = 0.9$ ,  $m = 200$ .

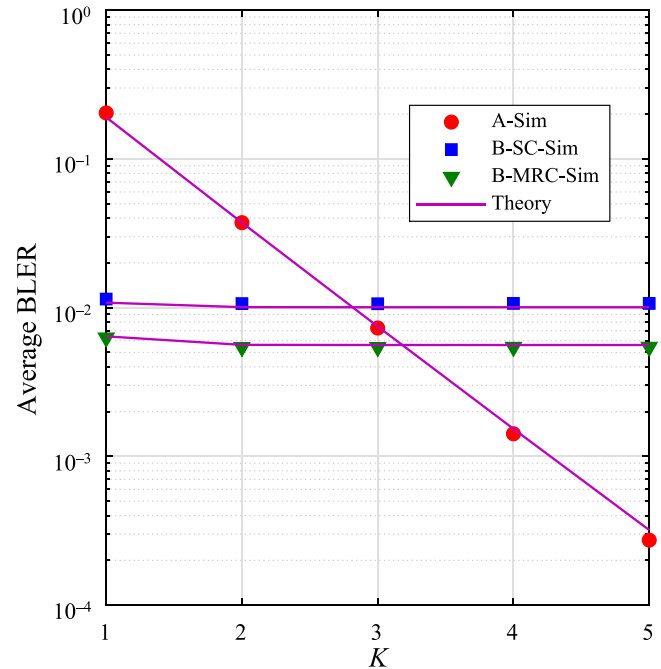


FIGURE 4 Average BLER at A and B as a function of  $K$  when  $\tilde{P}_S = 17.5$  dBm,  $\mu = 0.25$ ,  $a_2 = 0.8$ ,  $m = 300$ .

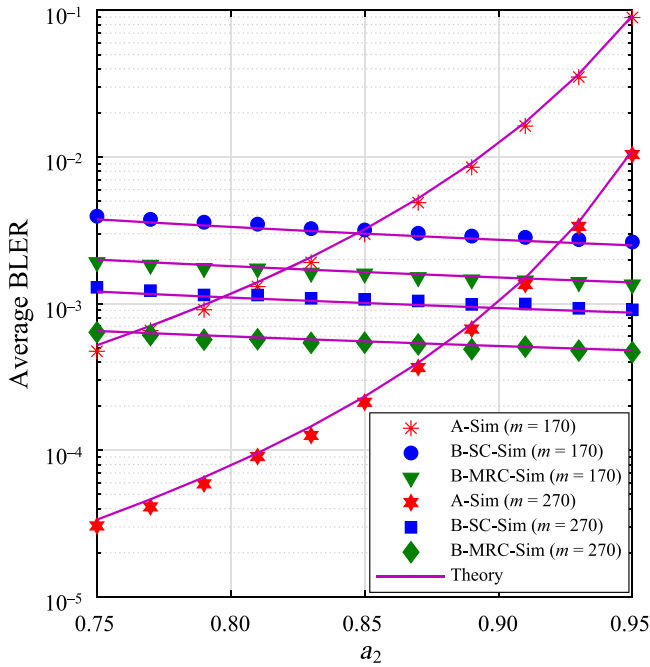


FIGURE 5 Average BLERs at A and B as a function of  $a_2$  when  $\bar{P}_S = 25$  dBm,  $\mu = 0.1$ ,  $K = 4$ .

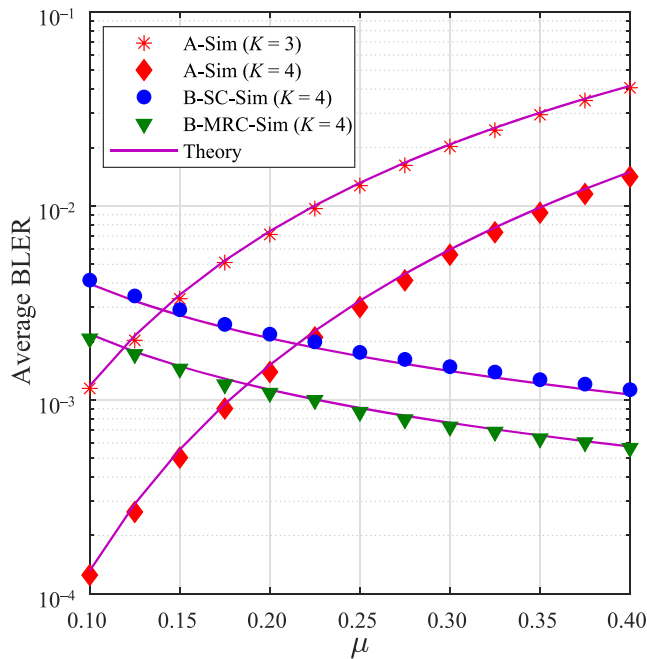


FIGURE 6 Average BLERs at A and B as a function of  $\mu$  when  $\bar{P}_S = 22.5$  dBm,  $a_2 = 0.8$ ,  $K = 3$ ,  $m = 250$ .

the A–B link is better. Therefore, the power ratio  $\mu$  or the transmit power  $\bar{P}_A$  needs to be designed carefully to obtain the required QoS and/or provide performance fairness between A and B. For example, if the required QoS

is that BLERs at A and B are lower than 0.01, with  $K = 4$  and SC is used at B, then from this figure, the BLER values at A and B are the same as  $\mu \approx 0.22$ .

## 6 | CONCLUSIONS

This paper presented the average BLER of the cooperative NOMA scheme using SPC, where the near user operates in the FD mode to assist in forwarding the desired signal to the far user over a flat Rayleigh fading channel. In the proposed scheme, the PRS method is employed to enhance the BLER performance at the selected near user, and the SC or MRC combiner is employed at the far user. We derived the closed-form expressions of the average BLERs for two users and then conducted Monte Carlo simulations to validate these derived expressions. The results showed that the far user obtained the diversity gain but that of the near user was zero. In addition, the PRS method significantly improves the performance of the selected near user. Finally, important system parameters, such as the fraction  $a_2$  and the transmit power of the near user, should be designed carefully to obtain the required QoS and ensure performance fairness between A and B.

## ACKNOWLEDGMENTS

The authors would like to thank Van Lang University, Vietnam, for funding this work.

## CONFLICT OF INTEREST STATEMENT

The authors declare that there are no conflicts of interest.

## ORCID

Ha Duy Hung  <https://orcid.org/0000-0001-6980-7273>

Tran Trung Duy  <https://orcid.org/0000-0002-3947-2174>

## REFERENCES

1. G. Durisi, T. Koch, and P. Popovski, *Toward massive, ultrareliable, and low-latency wireless communication with short packets*, Proc. IEEE **104** (2016), no. 9, 1711–1726.
2. Y. Polyanskiy, H. V. Poor, and S. Verdú, *Channel coding rate in the finite blocklength regime*, IEEE Trans. Inf. Theory **56** (2010), no. 5, 2307–2359.
3. L. Zhang and Y. Liang, *Average throughput analysis and optimization in cooperative IoT networks with short packet communication*, IEEE Trans. Veh. Technol. **67** (2018), no. 12, 11549–11562.
4. Y. Yang, Y. Song, and F. Cao, *HARQ assisted short-packet communications for cooperative networks over Nakagami- $m$  fading channels*, IEEE Access **8** (2020), 151171–151179.
5. L. Wei, Y. Yang, and B. Jiao, *Secrecy throughput in full-duplex multiuser MIMO short-packet communications*, IEEE Wireless Commun. Lett. **10** (2021), no. 6, 1339–1343.

6. C. D. Ho, T. V. Nguyen, T. Huynh-The, T. T. Nguyen, D. B. da Costa, and B. An, *Short-packet communications in wireless-powered cognitive IoT networks: performance analysis and deep learning evaluation*, *IEEE Trans. Veh. Technol.* **70** (2021), no. 3, 2894–2899.
7. C. Feng, H. M. Wang, and H. V. Poor, *Reliable and secure short-packet communications*, *IEEE Trans. Wireless Commun.* **21** (2022), no. 3, 1913–1926.
8. A. Agarwal, A. K. Jagannatham, and L. Hanzo, *Finite block-length non-orthogonal cooperative communication relying on SWIPT-enabled energy harvesting relays*, *IEEE Trans. Commun.* **68** (2020), no. 6, 3326–3341.
9. X. Lai, Q. Zhang, and J. Qin, *Cooperative NOMA short-packet communications in flat Rayleigh fading channels*, *IEEE Trans. Veh. Technol.* **68** (2019), no. 6, 6182–6186.
10. F. Salehi, N. Neda, M.-H. Majidi, and H. Ahmadi, *Cooperative NOMA-based user pairing for URLLC: a max-min fairness approach*, *IEEE Syst. J.* **16** (2021), no. 3, 3833–3843.
11. X. Lu, P. Wang, G. Li, D. Niyato, and Z. Li, *Short-packet backscatter assisted wireless-powered relaying with NOMA: mode selection with performance estimation*, *IEEE Trans. Cog. Commun. Netw.* **8** (2021), no. 1, 216–231.
12. C. Guo, C. Guo, S. Zhang, and Z. Ding, *Adaptive relaying protocol design and analysis for short-packet cooperative NOMA*, *IEEE Trans. Veh. Technol.* **72** (2022), 2689–2694.
13. T.-H. Vu, T.-V. Nguyen, Q.-V. Pham, D. B. da Costa, and S. Kim, *Short-packet communications for UAV-based NOMA systems under imperfect CSI and SIC*, *IEEE Trans. Cog. Commun. Netw.* **9** (2022), 463–478.
14. L. Yuan, Q. Du, and F. Fang, *Performance analysis of full-duplex cooperative NOMA short-packet communications*, *IEEE Trans. Veh. Technol.* **71** (2022), 13409–13414.
15. X. Sun, S. Yan, N. Yang, Z. Ding, C. Shen, and Z. Zhong, *Short-packet downlink transmission with non-orthogonal multiple access*, *IEEE Trans. Wireless Commun.* **17** (2018), no. 7, 4550–4564.
16. J. Zheng, Q. Zhang, and J. Qin, *Average block error rate of downlink NOMA short-packet communication systems in Nakagami-m fading channels*, *IEEE Commun. Lett.* **23** (2019), no. 10, 1712–1716.
17. X. Lai, Q. Zhang, and J. Qin, *Downlink NOMA networks with hybrid long-packet and short-packet communications in flat Rayleigh fading channels*, *IEEE Syst. J.* **14** (2019), 3410–3413.
18. S. Han, X. Xu, Z. Liu, P. Xiao, K. Moessner, X. Tao, and P. Zhang, *Energy-efficient short packet communications for uplink NOMA-based massive MTC networks*, *IEEE Trans. Veh. Technol.* **68** (2019), no. 12, 12066–12078.
19. Y. Gu, H. Chen, Y. Li, and B. Vucetic, *Ultra-reliable short-packet communications: half-duplex or full-duplex relaying?* *IEEE Wireless Commun. Lett.* **7** (2018), no. 3, 348–351.
20. X. Lai, T. Wu, Q. Zhang, and J. Qin, *Average secure BLER analysis of NOMA downlink short-packet communication systems in flat Rayleigh fading channels*, *IEEE Trans. Wireless Commun.* **20** (2020), no. 5, 2948–2960.
21. M. K. Simon and M.-S. Alouini, *Digital communications over fading channels [book review]*, *IEEE Trans. Inf. Theory* **54** (2008), no. 7, 3369–3370.
22. Y. Yu, H. Chen, Y. Li, Z. Ding, and B. Vucetic, *On the performance of non-orthogonal multiple access in short-packet communications*, *IEEE Commun. Lett.* **22** (2017), no. 3, 590–593.
23. H. D. Hung, T. T. Duy, P. N. Son, L. T. Thuong, and M. Voznak, *Security-reliability trade-off analysis for rateless codes-based relaying protocols using NOMA, cooperative jamming and partial relay selection*, *IEEE Access* **9** (2021), 131087–131108.
24. N. N. Tan, T. T. Duy, T. T. Phuong, M. Voznak, L. Xingwang, and H. V. Poor, *Security-reliability trade-off analysis for rateless codes-based relaying protocols using NOMA, cooperative jamming and partial relay selection*, *IEEE Trans. Veh. Technol.* **71** (2022), no. 6, 6173–6188.
25. Z. Zhang, Z. Ma, M. Xiao, Z. Ding, and P. Fan, *Full-duplex device-to-device-aided cooperative nonorthogonal multiple access*, *IEEE Trans. Veh. Technol.* **66** (2016), no. 5, 4467–4471.
26. U. Siddique, H. Tabassum, and E. Hossain, *Downlink spectrum allocation for in-band and out-band wireless backhauling of full-duplex small cells*, *IEEE Trans. Commun.* **65** (2017), no. 8, 3538–3554.
27. M. Vaezi, R. Schober, Z. Ding, and H. V. Poor, *Non-orthogonal multiple access: common myths and critical questions*, *IEEE Wireless Commun.* **26** (2019), no. 5, 174–180.
28. D. Bharadia, E. McMillin, and S. Katti, *Full duplex radios*, *Proc. Conf. ACM SIGCOMM*, 2013, pp. 375–386.
29. X. Wang, M. Jia, Q. Guo, I. W.-H. Ho, and F. C.-M. Lau, *Full-duplex relaying cognitive radio network with cooperative non-orthogonal multiple access*, *IEEE Syst. J.* **13** (2019), no. 4, 3897–3908.
30. B. Makki, T. Svensson, and M. Zorzi, *Finite block-length analysis of the incremental redundancy HARQ*, *IEEE Wireless Commun. Lett.* **3** (2014), no. 5, 529–532.
31. N. P. Le and K. N. Le, *Performance analysis of NOMA short-packet communications with QoS-based SIC detecting order*, *IEEE Wireless Commun. Lett.* **11** (2021), no. 3, 617–621.
32. Y. Yuan, Y. Xu, Z. Yang, P. Xu, and Z. Ding, *Energy efficiency optimization in full-duplex user-aided cooperative SWIPT NOMA systems*, *IEEE Trans. Commun.* **67** (2019), no. 8, 5753–5767.
33. G. A. Ropokis, A. A. Rontogiannis, and K. Berberidis, *BER performance analysis of cooperative DaF relay networks and a new optimal DaF strategy*, *IEEE Trans. Wireless Commun.* **10** (2011), no. 4, 1044–1049.
34. I. S. Gradshteyn and I. M. Ryzhik, *Table of integrals, series, and products*, Academic Press, San Diego, California, USA, 2014.

## AUTHOR BIOGRAPHIES



**Ha Duy Hung** received the B.S. and M.S. degrees in Electronics and Telecommunications Engineering from the Institute of Post and Telecommunication, Vietnam, University of Transport and Communications, Ha Noi, Vietnam, in 2007 and 2014. In 2017, he joined the Faculty of Electrical and Electronics Engineering at Ton Duc Thang University, Vietnam, as a lecturer. In 2021, he received a Ph.D. in Communication Technology at the VSB Technical University of Ostrava, Czech Republic. His major

interests are cooperative communications and physical-layer security. He can be contacted via email at haduyhung@tdtu.edu.vn.



**Hoang Van Toan** received the B.S. degree in Communication Command from Telecommunications University, Ministry of Defense, Nha Trang, Vietnam, in 2002, the B.Eng. degree in Electrical Engineering from Le Quy Don Technical University, Ha Noi, Vietnam, in 2006, M.Eng. degree in Electronics Engineering from Posts and Telecommunications, Institute of Technology, Ho Chi Minh City, Vietnam, in 2011 and the Ph.D. degree from Le Quy Don Technical University, Hanoi, Vietnam, in 2018. His research interests include cognitive radio, energy harvesting, NOMA, UAV, URLLC, and signal processing for wireless cooperative communications. He can be contacted via email at hoangvantoan@tcu.edu.vn.



**Tran Trung Duy** received the Ph.D. degree in Electrical Engineering from the University of Ulsan, Rep. of Korea. In 2013, he joined the Posts and Telecommunications Institute of Technology, Ho Chi Minh city Campus (PTIT-HCM) as a lecturer. Since 2022, he has been an associate professor of Wireless Communications at PTIT-HCM. Since 2021, he has been an associate editor for the Wireless Communications and Mobile Computing Journal, Frontiers in Communications and Networks Journal, and the Journal of Transportation Science and Technology. His major research interests include cooperative communications, cooperative multi-hop, cognitive radio, physical-layer security, energy harvesting, hardware impairments, and fountain codes. He can be contacted via email at duytt@ptit.edu.vn.



**Le The Dung** received the B.S. degree in Electronics and Telecommunication Engineering from Ho Chi Minh City University of Technology, Ho Chi Minh City, Vietnam, in 2008, and both the M.S. and Ph.D. degrees in Electronics and Computer Engineering from Hongik University, Seoul, Rep. of Korea, in 2012 and 2016, respectively. From 2007 to 2010, he worked at Signet Design

Solutions Vietnam as a Hardware Design Engineer. He worked with Chungbuk National University, Cheongju, Rep. of Korea as a Postdoctoral Research Fellow from May 2016 to December 2022. Since September 2022, he has been with FPT University, HCMC Campus, as a lecturer and researcher. At the same time, he has been with RMIT University Vietnam as a teaching assistant. He has published more than 80 papers in international journals and conferences. His major research interests include routing protocols, network coding, network stability analysis, optimization of mobile ad hoc networks, cognitive radio ad hoc networks, and visible light communication networks. He received the IEEE IS3C2016 Best Paper Award. He can be contacted via email at dunglt96@fe.edu.vn.



**Q. S. Vu** is a lecturer in the Faculty of Automotive Engineering, School of Technology, Van Lang University, Ho Chi Minh City, Vietnam. He received the B.E., M.S., and Ph.D. degrees in Electrical Engineering from Peter the Great St. Petersburg State Polytechnical University in 2012, 2014, and 2019, respectively. He can be contacted by email at Sy.vq@vlu.edu.vn.

**How to cite this article:** H. D. Hung, H. V. Toan, T. T. Duy, L. T. Dung, and Q. S. Vu, *On the block error rate performance of cooperative non-orthogonal multiple access short-packet communications with full-duplex relay and partial relay selection*, ETRI Journal **46** (2024), 446–460. DOI [10.4218/etrij.2023-0125](https://doi.org/10.4218/etrij.2023-0125).

## APPENDIX A: COMPUTING $\mathbb{E}\{\epsilon_{x_A}^{SA}\}$ AND $\mathbb{E}\{\epsilon_{x_B}^{SA}\}$

First, from (1), the CDF of  $|h_{SA}|^2$  can be expressed as

$$\begin{aligned} F_{|h_{SA}|^2}(x) &= \Pr\left(\max_{k=1,2,\dots,K} (|h_{SA_k}|^2) < x\right) \\ &= \prod_{k=1}^K F_{|h_{SA_k}|^2}(x) = \left(1 - e^{-\frac{x}{\lambda_{SA}}}\right)^K \\ &= 1 + \sum_{q=1}^K (-1)^q C_K^q e^{-\frac{qx}{\lambda_{SA}}}. \end{aligned} \quad (\text{A.1})$$

Combining (A.1) and (5), we have

$$\begin{aligned}
 F_{\gamma_{x_A}^{SA}}(x) &= \Pr\left(\frac{a_1 P_S |h_{SA}|^2}{P_A \lambda_{SI} + 1} < x\right) \\
 &= \Pr\left(|h_{SA}|^2 < \frac{x(P_A \lambda_{SI} + 1)}{P_S a_1}\right) \\
 &= 1 + \sum_{q=1}^K (-1)^q C_K^q e^{-q\phi_a x},
 \end{aligned} \tag{A.2}$$

where  $\phi_a = (P_A \lambda_{SI} + 1)/(P_S a_1 \lambda_{SA})$ .

Substituting  $F_{\gamma_{x_A}^{SA}}(x)$  into (15), after some manipulation, we obtain  $\mathbb{E}\{\epsilon_{x_A}^{SA}\}$  as in (17) as

$$\begin{aligned}
 \mathbb{E}\{\epsilon_{x_A}^{SA}\} &\approx \delta_a \sqrt{m} \int_{v_a}^{u_a} F_{\gamma_{x_A}^{SA}}(x) dx \\
 &\approx 1 + \sum_{q=1}^K (-1)^q C_K^q \frac{\delta_a \sqrt{m}}{q\phi_a} (e^{-q\phi_a v_a} - e^{-q\phi_a u_a}).
 \end{aligned} \tag{A.3}$$

We now derive the expression of  $\mathbb{E}\{\epsilon_{x_B}^{SA}\}$ . The CDF of  $\gamma_{x_B}^{SA}, F_{\gamma_{x_B}^{SA}}(x)$ , can be calculated as

$$\begin{aligned}
 F_{\gamma_{x_B}^{SA}}(x) &= \Pr\left(\frac{a_2 P_S |h_{SA}|^2}{a_1 P_S |h_{SA}|^2 + P_A \lambda_{SI} + 1} < x\right) \\
 &= \begin{cases} F_{|h_{SA}|^2}\left(\frac{x(P_A \lambda_{SI} + 1)}{a_1 P_S (u - x)}\right), & \text{if } x < u \\ 1, & \text{if } x \geq u \end{cases},
 \end{aligned} \tag{A.4}$$

where  $u = a_2/a_1$ .

Then, combining (A.4) and (15) yields

$$\mathbb{E}\{\epsilon_{x_B}^{SA}\} \approx \begin{cases} E_1 = 1 + \sum_{q=1}^K (-1)^q C_K^q \delta_b \sqrt{m} \int_{v_b}^{u_b} e^{-\frac{qx\phi_a}{u-x}} dx, & \text{if } u_b \leq u \\ E_2 = 1 + \sum_{q=1}^K (-1)^q C_K^q \delta_b \sqrt{m} \int_{v_b}^u e^{-\frac{qx\phi_a}{u-x}} dx, & \text{if } v_b \leq u < u_b \\ 1, & \text{if } u < v_b \end{cases} \tag{A.5}$$

Next, considering the integral in  $E_1$  in (A.5), we have

$$\begin{aligned}
 \int_{v_b}^{u_b} e^{-\frac{qx\phi_a}{u-x}} dx &= e^{q\phi_a} \int_{u-u_b}^{u-v_b} e^{-\frac{q\phi_a u}{t}} dt \\
 &= q\phi_a u e^{q\phi_a} \int_{\frac{q\phi_a u}{u-u_b}}^{\frac{q\phi_a u}{u-v_b}} \frac{1}{r^2} e^{-r} dr.
 \end{aligned} \tag{A.6}$$

Applying [34, eq. (2.325.2)] to calculate the integral in (A.6), we obtain

$$\begin{aligned}
 \int_{v_b}^{u_b} e^{-\frac{qx\phi_a}{u-x}} dx &= e^{q\phi_a} \left[ (u - v_b) e^{-\frac{q\phi_a u}{u-v_b}} - (u - u_b) e^{-\frac{q\phi_a u}{u-u_b}} \right] \\
 &+ q\phi_a u e^{q\phi_a} \left[ \text{Ei}\left(\frac{q\phi_a u}{v_b - u}\right) - \text{Ei}\left(\frac{q\phi_a u}{u_b - u}\right) \right].
 \end{aligned} \tag{A.7}$$

Substituting (A.7) into (A.5) yields

$$\begin{aligned}
 E_1 &= 1 + \sum_{q=1}^K (-1)^q C_K^q \delta_b \sqrt{m} e^{q\phi_a} \\
 &\times \left[ (u - v_b) e^{-\frac{q\phi_a u}{u-v_b}} - (u - u_b) e^{-\frac{q\phi_a u}{u-u_b}} \right] \\
 &+ \sum_{q=1}^K (-1)^q C_K^q \delta_b \sqrt{m} q\phi_a u e^{q\phi_a} \\
 &\times \left[ \text{Ei}\left(\frac{q\phi_a u}{v_b - u}\right) - \text{Ei}\left(\frac{q\phi_a u}{u_b - u}\right) \right].
 \end{aligned} \tag{A.8}$$

Next, using (A.7), we can calculate the integral in  $E_2$  in (A.5) as

$$\int_{v_b}^u e^{-\frac{qx\phi_a}{u-x}} dx = e^{q\phi_a} (u - v_b) e^{-\frac{q\phi_a u}{u-v_b}} + q\phi_a u e^{q\phi_a} \text{Ei}\left(\frac{q\phi_a u}{v_b - u}\right). \tag{A.9}$$

Substituting (A.9) into (A.5) yields

$$\begin{aligned}
 E_2 &= 1 + \sum_{q=1}^K (-1)^q C_K^q \delta_b \sqrt{m} e^{q\phi_a} \\
 &\times \left[ (u - v_b) e^{-\frac{q\phi_a u}{u-v_b}} + q\phi_a u \text{Ei}\left(\frac{q\phi_a u}{v_b - u}\right) \right].
 \end{aligned} \tag{A.10}$$

## APPENDIX B: COMPUTING $F_{\gamma_{x_B}^{MRC}}^L(\gamma)$ AND $F_{\gamma_{x_B}^{MRC}}^H(\gamma)$

Case 1:  $\gamma < u$ .

$$\begin{aligned}
 F_{\gamma_{x_B}^{MRC}}(\gamma) &= F_{\gamma_{x_B}^{MRC}}^L(\gamma) = \Pr\left(\frac{a_2 P_S |h_{SB}|^2}{a_1 P_S |h_{SB}|^2 + 1} + P_A |h_{AB}|^2 < \gamma\right) \\
 &= \int_0^{\frac{\gamma}{P_A}} \Pr\left(|h_{SB}|^2 < \frac{\gamma - P_A y}{P_S [a_2 - a_1 (\gamma - P_A y)]}\right) f_{|h_{AB}|^2}(y) dy \\
 &= 1 - e^{-\frac{\gamma}{P_A \lambda_{AB}}} - \frac{1}{\lambda_{AB}} e^{\frac{1}{P_S a_1 \lambda_{SB}} + \frac{u-\gamma}{P_A \lambda_{AB}}} \int_{\frac{u-\gamma}{P_A}}^{\frac{u}{P_S P_A a_1 \lambda_{SB} + \lambda_{AB}}} e^{-\frac{y}{P_S P_A a_1 \lambda_{SB} + \lambda_{AB}}} dy.
 \end{aligned} \tag{B.1}$$

Applying the Gaussian–Chebyshev quadrature approach for the integral in (B.1), after some manipulations, we obtain

$$F_{\gamma_{\text{SB}}}^L(\gamma) = 1 - e^{-\frac{\gamma}{P_A \lambda_{\text{AB}}}} - \frac{1}{2P_A \lambda_{\text{AB}}} \sum_{i=1}^N w_N \sqrt{1 - y_i^2} \gamma e^{\frac{\gamma(y_i-1)}{P_S a_1 \lambda_{\text{SB}} [\gamma(y_i-1)+2u]} - \frac{\gamma(y_i+1)}{2P_A \lambda_{\text{AB}}}}, \quad (\text{B.2})$$

where  $w_N = \pi/N$ ,  $y_i = \cos(\frac{2i-1}{2N}\pi)$ .

Case 2:  $\gamma > u$ .

$$F_{\gamma_{\text{SB}}}^{\text{MRC}}(\gamma) = F_{\gamma_{\text{SB}}}^H(\gamma) = \int_0^{\frac{\gamma-u}{P_A}} f_{|h_{\text{AB}}|^2}(y) dy - \int_{\frac{\gamma-u}{P_A}}^{\frac{\gamma}{P_A}} \Pr\left(|h_{\text{SB}}|^2 < \frac{\gamma - P_A y}{P_S [a_2 - a_1(\gamma - P_A y)]}\right) f_{|h_{\text{AB}}|^2}(y) dy. \quad (\text{B.3})$$

Letting  $t = y - \frac{\gamma-u}{P_A}$  for the second integral in (B.3), we obtain

$$F_{\gamma_{\text{SB}}}^H(\gamma) = 1 - \left(1 + \frac{\eta}{\lambda_{\text{AB}}} e^{\frac{1}{P_S a_1 \lambda_{\text{AB}}} + \frac{u}{P_A \lambda_{\text{AB}}}}\right) e^{-\frac{\gamma}{P_A \lambda_{\text{AB}}}}, \quad (\text{B.4})$$

where  $\eta = \int_0^{\frac{u}{P_A}} e^{-\frac{u}{P_S a_1 \lambda_{\text{SB}} t} - \frac{t}{\lambda_{\text{AB}}}} dt$  yields

$$\eta = \frac{u}{2P_A} \sum_{i=1}^N w_N \sqrt{1 - y_i^2} e^{-\frac{2}{P_S a_1 \lambda_{\text{SB}} (y_i+1)} - \frac{u(y_i+1)}{2P_A \lambda_{\text{AB}}}}. \quad (\text{B.5})$$